PHYSICAL REVIEW B **86**, 041202(R) (2012)

Mechanism for optical initialization of spin in NV$^-$ center in diamond

SangKook Choi, Manish Jain, and Steven G. Louie
Department of Physics, University of California, Berkeley, California 94720 and Materials Sciences Division, Lawrence Berkeley National Laboratory, Berkeley, California 94720

(Received 5 January 2012; revised manuscript received 27 March 2012; published 20 July 2012)

Optical initialization of the negatively charged nitrogen-vacancy (NV$^-$) center in diamond makes it one of the best candidates for realization of addressable spins in the solid state for quantum computing and other studies. However, its exact mechanism was not clear. We show that exact diagonalization of a many-electron Hamiltonian with parameters derived from *ab initio* GW calculations puts strong constraints on the mechanism. The energy surfaces of the low-energy many-body states and the relaxation processes of photoexcitation responsible for the optical initialization are calculated. Intersystem crossings are shown to be essential.

DOI: 10.1103/PhysRevB.86.041202 PACS number(s): 71.15.Qe, 61.72.jn, 71.10.Fd, 71.15.Mb

The negatively charged nitrogen-vacancy (NV$^-$) center in diamond is a defect complex composed of a substitutional nitrogen atom and an adjacent carbon vacancy[1,2] as shown in Fig. 1(a). The NV$^-$ center has emerged as one of the candidates for realization of individually addressable spins in the solid state for quantum computing and other studies.[3–12] The interest in this system in large part stems from an optical initialization process under ambient conditions, which results in a state with long spin coherence time of up to $\sim$1 ms.[13] The optical initialization of the NV$^-$ center, which starts with a degenerate mixed triplet ground state, involves optical transition to an excited state and subsequent relaxations to the ground state with an unentangled pure spin of $m_s = 0$. The electronic structure of the low-energy excited states, especially the placement of possible singlet defect levels with respect to the ground ($^3A_2$) and first excited triplet (^3E) levels, is crucial in explaining the optical initialization mechanism. However, up to now there is no consensus. It is reported experimentally that two singlet levels ($^1A_1$ and ^1E) are near the ground and the first excited triplet levels, but the character and ordering of the two singlet levels are not determined.[14,15] Various theoretical studies also failed to agree with each other.[16–22] The most widely used picture, where one singlet level ($^1A_1$) is assumed to lie in between the two lowest-lying triplet levels,[23–25] has not been confirmed. There exist two different "two active singlet level" models[15–17] involving an intermediate step of radiative decay between two singlet levels of $^1A_1$ and ^1E before the system decays to the ground state. However these models are in contradiction with the experimental findings that after the initially excited triplet level decayed to a singlet state, the system decays nonradiatively.[14,15]

The theoretical difficulty in determining the nature of this system arises from the fact that the NV$^-$ center is a deep-level center in the band gap of diamond with multiple localized, interacting electrons. Such systems are not appropriate for the mean-field type of calculations because of strong electron-electron interaction. Mimicking the system as a small isolated diamond cluster with a NV$^-$ center is also expected to be not so appropriate because it does not include the large screening effects from the bulk and because of issues with possible spurious boundary effects. Furthermore, this defect is prone to large excited-state structural relaxation.[16,19,26] An effective model Hamiltonian with reliable interaction parameters for the electrons, such as an extended Hubbard model, offers an efficient way to evaluate the excited-state level structure which could include many-electron interactions fully if solved exactly. In such models, the electron-electron interaction and screening effect of the host material must be accurately incorporated using effective Coulomb interaction parameters. The effects of structural relaxation should also be taken into account through the parameters. Such approaches had been hindered in the past by the difficulty in getting physically grounded model parameters.

In this study, we employ an extended Hubbard model Hamiltonian with structure-dependent interaction parameters that are derived from *ab intio* quasiparticle energy levels. These parameters are put on physical grounds by fitting the quasiparticle energies of the model system to those of the real system, both calculated within the same GW approximation to the electron self-energy operator.[27,28] The idea is to use relevant physical quantities, and a sufficient number of them, to determine the effective interactions.

For the real system, we calculated from first principles the ground state using density functional theory in the local spin density approximation (DFT-LSDA) and the low-energy excited-state quasiparticle levels using the *ab initio* GW method.[29] Our *ab initio* GW quasiparticle level diagram at the ground-state equilibrium geometry (GEG) of the NV$^-$ center is shown in Fig. 1(b). There are 8 quasiparticle defect states near the band gap. These defect states, which are localized at the defect site, should form an efficient basis set for describing the low-energy charge-conserved excitations that are of the main interest of the present study.

We chose the Hilbert space for the effective model system to be spanned by the 8 dangling-bond spin orbitals at the 3 carbon atoms and the one nitrogen atom nearest to the vacancy site.[30] To ensure that such a basis would describe the lowest lying excitations well, we constructed maximally localized Wannier functions (MLWFs) from the above mentioned *ab initio* 8 defect states.[31] As is evident from Fig. 2, the MLWFs are strongly localized at the atoms nearest to the vacancy, showing dangling bond characteristics. It also shows that hybridization of the u states and the extended state in the valence band is small. Simple electron counting dictates that 6 electrons be shared among these 8 spin orbitals for the NV$^-$ center: 3 from the 3 carbon atoms, 2 from the nitrogen atom, and 1 from

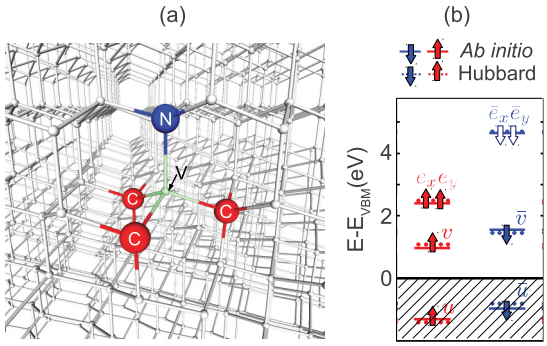

FIG. 1. (Color online) (a) Ground-state structure. Carbon (nitrogen) atoms nearest to the vacancy site (V) are marked by atomic symbol C (N). (b) Quasiparticle energy levels near the band gap, from *ab initio* GW calculation (solid line) of a NV^- center and from GW calculation of the extended Hubbard model (dotted line). The filled and open arrows correspond to quasihole and quasiparticle state (i.e., removing and adding an electron to the system), respectfully. For each spin, these levels belong to the two A_1 and one E representation in C_{3v} symmetry group. We label them as $u(\bar{u})$, v $(\bar{v})$, e_x $(\bar{e}_x)$, and e_y $(\bar{e}_y)$ for up (down) spin states, marked by upward arrows and downward arrows.

the defect being negative charged. The effective Hamiltonian hence is taken as

$$H = \sum_{i\sigma} E_i n_{i\sigma} + \sum_{\substack{i\neq j\\ \sigma}} t_{ij} c^\dagger_{i\sigma} c_{j\sigma} + \sum_i U n_{i\uparrow} n_{i\downarrow} + \sum_{\substack{i>j\\ \sigma\sigma'}} V n_{i\sigma} n_{j\sigma'} \quad (1)$$

where $c^\dagger_{i\sigma}$, $c_{i\sigma}$, and $n^\dagger_{i\sigma}$ are creation, annihilation, and number operators at the site i with spin σ. It should be noted that while this model does not include all possible electron-electron interaction terms in the exact many-body Hamiltonian, it includes the two dominant terms when the Hilbert space is spanned by an atom-centered basis set,[32] namely, the on-site Coulomb repulsion (U) as well as the nearest-neighbor Coulomb repulsion (V) term. Further simplifications have been made. As shown in Fig. 2, the Wannier functions centered at the carbon atoms and the nitrogen atom are all similar

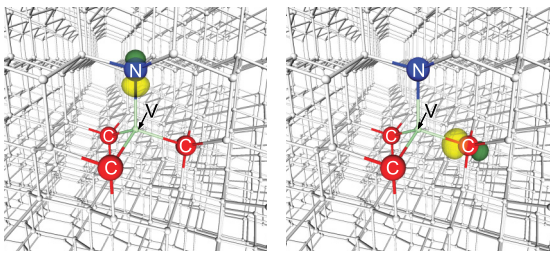

FIG. 2. (Color online) Defect-state Wannier functions. Isosuface plot of spin-up Wannier functions at amplitude $W(\vec{r}) = \pm|W(\vec{r})|_{\max} \times 0.5$, constructed from the 4 spin-up defect states in Fig. 1(b). Yellow or light-gray (green or dark gray) color denotes plus (minus) sign of the amplitude. The Wannier functions centered at each carbon are equivalent, so only one of them is shown.

TABLE I. Extended Hubbard model parameters at the ground-state equilibrium geometry (GEG) and the optically excited-state equilibrium geometry (EEG).

Parameters (eV)	$E_C - E_N$	t_{NC}	t_{CC}	U	V
GEG	2.56	−0.68	−1.03	3.43	0.83
EEG	2.86	−0.75	−0.90	3.45	0.67

in shape and size. Their mean radii, which are defined as $\sqrt{\langle W|\,|\vec{r}|^2\,|W\rangle - |\langle W|\vec{r}|W\rangle|^2}$ where $\vec{r}$ is the position operator, are within 5% of one another. The mean radius is 2.0 Å for the up-spin orbital of nitrogen, 1.9 Å for the up-spin orbital of carbon, 1.9 Å for the down-spin orbital of nitrogen, and 1.8 Å for the down-spin orbital of carbon.

Based on this, we constrain that U for carbon and nitrogen are the same, and that the carbon-nitrogen V and carbon-carbon V are also all the same. We determined the parameters in Eq. (1) by comparing the quasiparticle energies calculated within the *ab initio* GW approach to those from a GW calculation of our model Hamiltonian at the GEG. To calculate the quasiparticle energies for the extended Hubbard model, we use the DFT-LSDA as the mean-field starting point.[33–35] We calculated the quasiparticle self-energy correction to the mean-field solution within the GW approximation. This is exactly the same level of approximation as the *ab initio* GW quasiparticle calculation for the real system. We tuned the model parameters until we minimize the differences between the model Hamiltonian quasiparticle energies and the *ab initio* quasiparticle energies. As seen in Fig. 1(b), the quasiparticle energies from our extended Hubbard model match the *ab initio* values to within 0.1 eV.

The parameters in Table I are physically well determined because the two Hamiltonians (model and real) are treated in equal footing with important self-energy effects incorporated. Because nitrogen has a larger atomic number than carbon, as expected, $E_C - E_N > 0$. t_{NC} and t_{CC} are close to a value from a MLWF analysis (∼−0.7 eV). U is also reasonable; the bare on-site Coulomb repulsion of π electrons in the carbon nanotube is ∼16 eV[36] but for the NV^- center it is screened by the diamond dielectric constant of 5.5.[37]

To understand the optical initialization process, it is important to include geometrical relaxation around the NV^- center in an excited state. To account for this Frank-Condon effect, we first calculated the excited-state equilibrium geometry (EEG) for the ^3E state of the NV^- center within an *ab initio* constrained DFT framework by depopulating the $\bar{v}$ level and populating either the $\bar{e}_x$ or $\bar{e}_y$ level.[29] At the EEG, N moves toward the vacancy by 0.05 Å while the three C nearest to the vacancy move outwards from the vacancy by 0.06 Å. We reevaluated the model parameters following the same procedure as for the GEG. Because the structural change between GEG and EEG is small [Fig. 3(a)], we may assume that the minimum-energy path between the two geometries can be explored by using parameters that are linear interpolations of the values from the two end points (GEG and EEG). The parameters at EEG are given in Table I.

Having parameterized the model Hamiltonian, we calculated the many-body eigenstates and their energies by exact

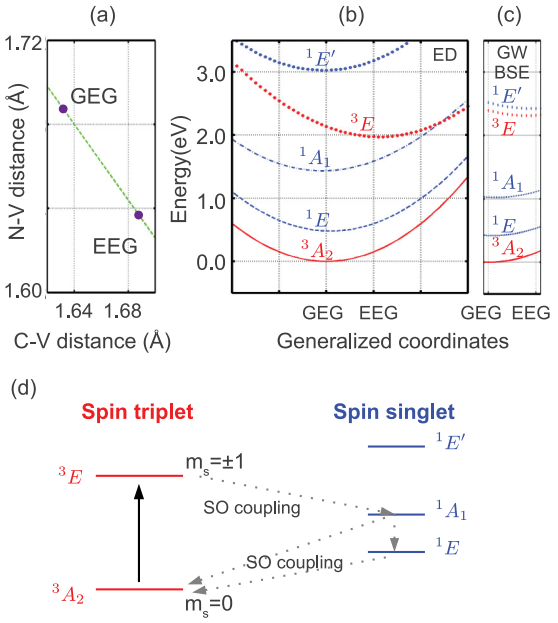

FIG. 3. (Color online) (a) Relaxation path taken between the GEG and EEG. (b) Energy surfaces from exact diagonalization of the extended Hubbard model. (c) Energy surfaces from a GW-BSE calculation of the extended Hubbard model. (d) Optical spin initialization mechanism supported by results from exact diagonalization of the extended Hubbard model.

diagonalization (or, in quantum chemistry language, a full CI calculation) of the Hamiltonian in the basis of all possible 6-electron Slater determinants spanned by the 8 spin orbitals. It is worth pointing out that exact diagonalization includes all many-electron correlation effects within our restricted Hilbert space. This is important because $U/t > 3$ in this system. Figure 3(b) shows the energy surfaces of the ground and excited states of the extended Hubbard model. As discussed in Ref. 29, in the range of generalized coordinates considered, the many-body states listed in Table II are ordered (from low to high energies) as $^3A_2$, ^1E, and $^1A_1$ in the e^2 hole configuration, and ^3E and ^1E in the v^1e^1 hole configuration.[21,22] Without any free parameters, our calculated many-body energy level differences for the triplet states match very well with experimental findings: (i) $E^{^3E}_{GEG} - E^{^3A_2}_{GEG} = 2.1$ eV, as compared to experimental vertical absorption energy of 2.2 eV. (ii) $E^{^3E}_{EEG} - E^{^3A_2}_{EEG} = 1.8$ eV, as compared to experimental vertical emission energy of 1.8 eV. (iii) A zero phonon line $E^{^3E}_{EEG} - E^{^3A_2}_{GEG} = 2.0$ eV, as compared to the experimental value of 1.945 eV.[1]

Figure 3(b) shows that the ordering of ^3E and $^1A_1$ levels is inverted as the system relaxes beyond EEG. This inversion of the ordering allows for the possibility of an intersystem crossing between these states. If intersystem crossing is mediated by spin-orbit coupling, which is known as the only mechanism to couple many-body states of different spin multiplicities in this system,[21,22] only the ^3E state with A_1 representation ($m_s = \pm 1$) can couple to $^1A_1$ as shown in Table II. These findings explain the observed optical initialization from the $m_s = \pm 1$ excited triplet state. Our results are distinctly different from those from a recent *ab initio* GW-BSE study,[16] where a level crossing between the ^3E and $^1E'$ levels is reported and there is no crossing between the ^3E and $^1A_1$ levels. We also computed the excited-state energies within the same GW-BSE approximation for the extended Hubbard model in the same 8-spin-orbital Hilbert space. Our GW-BSE results for the extended Hubbard model in Fig. 3(c) show that the ^3E and $^1E'$ levels are very close within the GW-BSE approach, reproducing the *ab initio* GW-BSE results. The difference between the results from

TABLE II. Low-lying many-body states of the NV^- center denoted by hole occupations and their symmetry representations (degenerate representation without spin-orbit coupling and corresponding spin-orbit split representations). Instead of electron occupation of single-particle orbitals, one can equivalently express a many-body state by hole occupation. Each ket vector represents a 6-orbital Slater determinant in second-quantized notation, for example, $c_a c_b|f\rangle = |ab\rangle$, where $|f\rangle$ is the 8-orbital Slater determinant.

	Sym. Rep.		
Hole Occ.	w/o SO	SO	Many-body States
v^1e^1	$^1E'$	E_x	$1/\sqrt{2}\|v\bar{e}_x\rangle - 1/\sqrt{2}\|\bar{v}e_x\rangle$
		E_y	$1/\sqrt{2}\|v\bar{e}_y\rangle - 1/\sqrt{2}\|\bar{v}e_y\rangle$
	^3E	E_x	$1/2\|ve_x\rangle - 1/2\|\bar{v}\bar{e}_x\rangle - i/2\|ve_y\rangle + i/2\|\bar{v}\bar{e}_y\rangle$
		E_y	$-1/2\|ve_x\rangle + 1/2\|\bar{v}\bar{e}_x\rangle + i/2\|ve_y\rangle + i/2\|\bar{v}\bar{e}_y\rangle$
		E_x	$1/\sqrt{2}\|v\bar{e}_y\rangle + 1/\sqrt{2}\|\bar{v}e_y\rangle$
		E_y	$1/\sqrt{2}\|v\bar{e}_x\rangle + 1/\sqrt{2}\|\bar{v}e_x\rangle$
		A_2	$1/2\|ve_x\rangle - 1/2\|\bar{v}\bar{e}_x\rangle + i/2\|ve_y\rangle + i/2\|\bar{v}\bar{e}_y\rangle$
		A_1	$1/2\|ve_x\rangle + 1/2\|\bar{v}\bar{e}_x\rangle + i/2\|ve_y\rangle - i/2\|\bar{v}\bar{e}_y\rangle$
e^2	$^1A_1$	A_1	$1/\sqrt{2}\|e_x\bar{e}_x\rangle + 1/\sqrt{2}\|e_y\bar{e}_y\rangle$
	^1E	E_x	$1/\sqrt{2}\|e_x\bar{e}_x\rangle - 1/\sqrt{2}\|e_y\bar{e}_y\rangle$
		E_y	$1/\sqrt{2}\|e_x\bar{e}_y\rangle - 1/\sqrt{2}\|\bar{e}_xe_y\rangle$
	$^3A_2$	E_x	$1/\sqrt{2}\|e_xe_y\rangle - 1/\sqrt{2}\|\bar{e}_x\bar{e}_y\rangle$
		E_y	$1/\sqrt{2}\|e_xe_y\rangle + 1/\sqrt{2}\|\bar{e}_x\bar{e}_y\rangle$
		A_1	$1/\sqrt{2}\|e_x\bar{e}_y\rangle + 1/\sqrt{2}\|\bar{e}_xe_y\rangle$

conventional GW-BSE and exact diagonalization arises from (i) the number of configurations (Slater determinants) to describe the many-electron states, and (ii) how these two methods treat electron-electron interaction. The conventional GW-BSE approach takes only one, e.g., the $|e_x e_y\rangle$ configurations out of the threefold degenerate ground state ($^3A_2$) configurations of $|e_x e_y\rangle$, $|\bar{e}_x \bar{e}_y\rangle$, and $1/\sqrt{2}|e_x \bar{e}_y\rangle + 1/\sqrt{2}|\bar{e}_x e_y\rangle$ in Table II. Then it considers single-electron-hole excitation and deexcitation from them. Due to this less complete description, the number of configurations composing a particular state within the GW-BSE calculation is smaller than the actual number of configurations from an exact diagonalization calculation. For instance, if one considers the ^3E representation in Table II, exact diagonalization would give rise to states mixing all 6 configurations ($|ve_x\rangle$, $|\bar{v}\bar{e}_x\rangle$, $|ve_y\rangle$, $|\bar{v}\bar{e}_y\rangle$, $1/\sqrt{2}|v\bar{e}_y\rangle + 1/\sqrt{2}|\bar{v}e_y\rangle$, $1/\sqrt{2}|v\bar{e}_x\rangle + 1/\sqrt{2}|\bar{v}e_x\rangle$). However, within GW-BSE, the ^3E states would consist of two configurations ($|ve_x\rangle$ and $|ve_y\rangle$) and are twofold degenerate. As for the treatment of interactions, standard GW-BSE method being a perturbative approach is an approximation to exact diagonalization in several ways for a given Hamiltonian. Conceptually, it does not include the vertex contribution in evaluating the electron self-energy, and the electron-hole interaction kernel in the Bethe-Salpeter equation is taken at the GW level.

While knowing the excited-state level positions is a necessary requirement of any model that would explain optical initialization, they are of themselves not sufficient. To have a complete understanding of the process, it is also important to calculate the transition rate between the many-body states. Our calculations lead to the following optical initialization mechanism shown in Fig. 3(d). First, an electron is excited radiatively from the $^3A_2$ ground-state level to the ^3E level; both are spin triplet states. Second, the $^1A_1(m_s = \pm 1)$ state in the ^3E level is deexcited to the $^1A_1$ level by an intersystem crossing mediated by spin-orbit coupling. For the last step, two paths are possible. One possible transition path to the final ground state is an intersystem crossing mediated by spin-orbit interaction[21,22] from $^1A_1$ to the $m_s = 0$ state of the ground-state $^3A_2$ level. The other possible path to the final ground state is first a nonradiative transition from $^1A_1$ to ^1E by electron–multiple-phonon interaction and a subsequent intersystem crossing transition from the ^1E level to the $m_s = 0$ state of $^3A_2$ by spin-orbit coupling, enabled by dynamic-Jahn-Teller-effect-assisted symmetry lowering of the structure from C_{3V} to C_{1h}.[22]

The proposed mechanism is supported by agreement of the calculated transition rates with the corresponding measured values. The $^3E \rightarrow {}^3A_2$ radiative deexcitation lifetime is calculated to be 20 ns using our calculated many-body states and within the electric dipole approximation, as compared to the experimental value of 13 ns.[29] The intersystem crossing rate between ^3E and $^1A_1$, mediated by spin-orbit coupling, is calculated to be ~50 ns within a displaced harmonic oscillator model (similar to the Marcus theory for electron transfer reaction[29]), as compared to the experimental value of 30 ns.[25] Radiative deexcitation from the $^1A_1$ state to the lower singlet state of ^1E is calculated to be ~70 ns, which is much larger than the reported lifetime of 1 ns.[14] It is consistent with the experimental observation that deexcitation from the singlet level (that the system in the initially optically excited triplet state decayed nonradiatively to; in our model it is $^1A_1$) is dominated by nonradiative transition.[14,15] We therefore assign that the deexcitation from $^1A_1$ is dominated by nonradiative transition. A definitive calculation of the rate of the last step of this mechanism is beyond our current model. The overall process nevertheless explains all the steps consistently with experiments in the optical initialization to the $m_s = 0$ ground state.

To conclude, we have constructed a theoretical model to understand the physical mechanism for the optical initialization of spin of the NV^- center in diamond. Using exact diagonalization of an extended Hubbard Hamiltonian determined from *ab initio* GW calculations, we incorporated full electron-electron interactions, the diamond host screening, and geometrical relaxation effects in the calculation. The computed ground- and excited-state energy surfaces and transition rates between them provided a consistent picture with experiments in support of an optical initialization path of $^3A_2 \rightarrow {}^3E \rightarrow {}^1A_1 \rightarrow {}^3A_2$ or $^3A_2 \rightarrow {}^3E \rightarrow {}^1A_1 \rightarrow {}^1E \rightarrow {}^3A_2$ in which intersystem crossings play a crucial role. Our method should be applicable to other deep centers in large band gap materials.

We thank A. Gali, F. Yang, and D.-H. Lee for fruitful discussions. S.C. acknowledges support from National Science Foundation Grant No. DMR10-1006184. M.J. is supported by the Director, Office of Science, Office of Basic Energy Sciences, Materials Sciences and Engineering Division, US Department of Energy under Contract No. DE-AC02-05CH11231. S.C. also acknowledges support from the Samsung Foundation. Computational resources have been provided by NSF through TeraGrid resources at NICS and DOE at Lawrence Berkeley National Laboratory's NERSC facility.

[1] G. Davies and M. F. Hamer, Proc. R. Soc. London A **348**, 285 (1976).

[2] A. Gruber, A. Dräbenstedt, C. Tietz, L. Fleury, J. Wrachtrup, and C. von Borczyskowski, Science **276**, 2012 (1997).

[3] F. Jelezko, T. Gaebel, I. Popa, M. Domhan, A. Gruber, and J. Wrachtrup, Phys. Rev. Lett. **93**, 130501 (2004).

[4] R. J. Epstein, F. M. Mendoza, Y. K. Kato, and D. D. Awschalom, Nat. Phys. **1**, 94 (2005).

[5] L. Childress, M. V. Gurudev Dutt, J. M. Taylor, A. S. Zibrov, F. Jelezko, J. Wrachtrup, P. R. Hemmer, and M. D. Lukin, Science **314**, 281 (2006).

[6] M. V. G. Dutt, L. Childress, L. Jiang, E. Togan, J. Maze, F. Jelezko, A. S. Zibrov, P. R. Hemmer, and M. D. Lukin, Science **316**, 1312 (2007).

[7] R. Hanson, V. V. Dobrovitski, A. E. Feiguin, O. Gywat, and D. D. Awschalom, Science **320**, 352 (2008).

[8]G. D. Fuchs, V. V. Dobrovitski, D. M. Toyli, F. J. Heremans, and D. D. Awschalom, Science **326**, 1520 (2009).

[9]G. D. Fuchs, V. V. Dobrovitski, D. M. Toyli, F. J. Heremans, C. D. Weis, T. Schenkel, and D. D. Awschalom, Nat. Phys. **6**, 668 (2010).

[10]B. B. Buckley, G. D. Fuchs, L. C. Bassett, and D. D. Awschalom, Science **330**, 1212 (2010).

[11]J. M. Taylor, P. Cappellaro, L. Childress, L. Jiang, D. Budker, P. R. Hemmer, A. Yacoby, R. Walsworth, and M. D. Lukin, Nat. Phys. **4**, 810 (2008).

[12]F. Dolde, H. Fedder, M. W. Doherty, T. Nobauer, F. Rempp, G. Balasubramanian, T. Wolf, F. Reinhard, L. C. L. Hollenberg, F. Jelezko, and J. Wrachtrup, Nat. Phys. **7**, 459 (2011).

[13]G. Balasubramanian, P. Neumann, D. Twitchen, M. Markham, R. Kolesov, N. Mizuochi, J. Isoya, J. Achard, J. Beck, J. Tissler, V. Jacques, P. R. Hemmer, F. Jelezko, and J. Wrachtrup, Nat. Mater. **8**, 383 (2009).

[14]V. M. Acosta, A. Jarmola, E. Bauch, and D. Budker, Phys. Rev. B **82**, 201202 (2010).

[15]L. J. Rogers, S. Armstrong, M. J. Sellars, and N. B. Manson, New J. Phys. **10**, 103024 (2008).

[16]Y. Ma, M. Rohlfing, and A. Gali, Phys. Rev. B **81**, 041204 (2010).

[17]P. Delaney, J. C. Greer, and J. A. Larsson, Nano Lett. **10**, 610 (2010).

[18]A. Ranjbar, M. Babamoradi, M. Heidari Saani, M. A. Vesaghi, K. Esfarjani, and Y. Kawazoe, Phys. Rev. B **84**, 165212 (2011).

[19]A. Gali, M. Fyta, and E. Kaxiras, Phys. Rev. B **77**, 155206 (2008).

[20]A. Lenef and S. C. Rand, Phys. Rev. B **53**, 13441 (1996).

[21]J. R. Maze, A. Gali, E. Togan, Y. Chu, A. Trifonov, E. Kaxiras, and M. D. Lukin, New J. Phys. **13**, 025025 (2011).

[22]M. W. Doherty, N. B. Manson, P. Delaney, and L. C. L. Hollenberg, New J. Phys. **13**, 025019 (2011).

[23]J. H. N. Loubser and J. A. van Wyk, Rep. Prog. Phys. **41**, 1201 (1978).

[24]A. P. Nizovtsev, S. Y. Kilin, F. Jelezko, I. Popa, A. Gruber, and J. Wrachtrup, Physica B **340–342**, 106 (2003).

[25]N. B. Manson, J. P. Harrison, and M. J. Sellars, Phys. Rev. B **74**, 104303 (2006).

[26]A. Gali, E. Janzén, P. Deák, G. Kresse, and E. Kaxiras, Phys. Rev. Lett. **103**, 186404 (2009).

[27]M. S. Hybertsen and S. G. Louie, Phys. Rev. B **34**, 5390 (1986).

[28]J.-L. Li, G.-M. Rignanese, E. K. Chang, X. Blase, and S. G. Louie, Phys. Rev. B **66**, 035102 (2002).

[29]See Supplemental Material at http://link.aps.org/supplemental/10.1103/PhysRevB.86.041202 for the details of the *ab initio* GW calculation, Hubbard model calculation, the ordering of lowest-lying many-body levels, and transition lifetime calculation (Refs. 38–47).

[30]J. H. N. Loubser and J. A. van Wyk, *Diamond Research*, Vol. 11 (Industrial Diamond Information Bureau, 1977).

[31]A. A. Mostofi, J. R. Yates, Y.-S. Lee, I. Souza, D. Vanderbilt, and N. Marzari, Comput. Phys. Commun. **178**, 685 (2008).

[32]P. W. Phillips, *Advanced Solid State Physics* (Westview Press, 2003).

[33]A. Svane and O. Gunnarsson, Phys. Rev. B **37**, 9919 (1988).

[34]J. A. Majewski and P. Vogl, Phys. Rev. B **46**, 12219 (1992).

[35]Y. Xie, R. Han, and X. Zhang, Phys. Rev. B **58**, 12721 (1998).

[36]C. D. Spataru, S. Ismail-Beigi, R. Capaz, and S. G. Louie, in *Carbon Nanotubes: Advanced Topics in the Synthesis, Structure, Properties and Applications*, edited by A. Jorio, G. Dresselhaus, and M. S. Dresselhaus (Springer, Berlin, 2008).

[37]C. Kittel, *Introduction to Solid State Physics* (Wiley, New York, 2005).

[38]See http://www1.nersc.gov/projects/paratec.

[39]F. M. Hossain, M. W. Doherty, H. F. Wilson, and L. C. L. Hollenberg, Phys. Rev. Lett. **101**, 226403 (2008).

[40]See http://www.berkeleygw.org.

[41]O. Svelto, *Principles of Lasers* (Springer, New York, 2009).

[42]A. Gali, T. Simon, and J. E. Lowther, New J. Phys. **13**, 025016 (2011).

[43]P. Scherer and S. F. Fischer, *Theoretical Molecular Biophysics* (Springer, New York, 2009).

[44]J. Jortner, J. Chem. Phys. **64**, 4860 (1976).

[45]V. Balzani, A. Juris, M. Venturi, S. Campagna, and S. Serroni, Chem. Rev. **96**, 759 (1996).

[46]D. Beljonne, Z. Shuai, G. Pourtois, and J. L. Bredas, J. Phys. Chem. A **105**, 3899 (2001).

[47]S. Mukamel, *Principles of Nonlinear Optical Spectroscopy* (Oxford University Press, New York, 1999).